Since January 2020 Elsevier has created a COVID-19 resource centre with free information in English and Mandarin on the novel coronavirus COVID-19. The COVID-19 resource centre is hosted on Elsevier Connect, the company's public news and information website.

Elsevier hereby grants permission to make all its COVID-19-related research that is available on the COVID-19 resource centre - including this research content - immediately available in PubMed Central and other publicly funded repositories, such as the WHO COVID database with rights for unrestricted research re-use and analyses in any form or by any means with acknowledgement of the original source. These permissions are granted for free by Elsevier for as long as the COVID-19 resource centre remains active.

Computer Methods and Programs in Biomedicine 200 (2021) 105843

Contents lists available at ScienceDirect

Computer Methods and Programs in Biomedicine

journal homepage: www.elsevier.com/locate/cmpb

SARS-CoV-2 droplet deposition path and its effects on the human upper airway in the oral inhalation

Hamed Mortazavi[a], Hamidreza Mortazavy Beni[a,*], Fatemeh Aghaei[b], Seyed Hossein Sajadian[a]

[a] Department of Biomedical Engineering, Arsanjan Branch, Islamic Azad University, Arsanjan, Iran
[b] Department of Immunology, Shiraz University of Medical Sciences, Shiraz, Iran

ARTICLE INFO

Article history:
Received 8 September 2020
Accepted 11 November 2020

Key words:
Micro-droplet
droplet tracking
coronavirus
human upper airway

ABSTRACT

Background and Objective: It is crucial to study the uptake of viral droplets in the human respiratory system to control, prevent, and treat diseases.

Methods: In this study, a well-verified real anatomical model was used; the passage of air in the human upper respiratory system computed using high-quality Computer Tomography (CT) images. Then, the airflow field, along with the coronavirus micro-droplets injection, was examined in this realistic model using the Fluid-Structure Interaction (FSI) method. The Discrete Phase Model (DPM) was used to solve the field, and with the help of it, the accurate assessment of the temporal and spatial motion of the deposition in the virus-impregnated droplets was obtained in vitro in the upper respiratory system.

Results: The results show that the amount of deposited micro-droplets in the nasal cavity area is meager at the inhalation only through the oral. However, it has the most residence time in this area. The most and least droplet absorption occurred in the oral cavity and larynx-trachea, respectively. Deposition efficiency is about 100% in 30 L/min flow rate and 10 μm diameter; in other words, no droplet enters the lungs. This study's other achievements include the relatively inverse relationship between droplets deposition efficiency in some parts of the upper airway, which have the most deformation in the tract.

Conclusions: Utilization of a realistic model with accurate and precise computational analysis can end speculation about the deposition zone, accumulation, and the effects of the COVID-19 virus on the upper respiratory tract. On the other hand, recognizing the virus-containing droplet location can ease understanding the areas where the virus can first infect in the upper respiratory tract.

© 2020 Elsevier B.V. All rights reserved.

1. Introduction

Coronavirus was first identified in 1965, with an average size of 0.15-0.08 μm [1]. With the help of high-sensitivity laser cameras, researchers have found that even in regular conversations, viral droplets can float in the air for a long time. Moreover, micro-droplets with diameter smaller than 5 μm can also be easily transmitted through inhalation to other people's airways in longer paths [2].

Coronavirus belongs to the large, positive, and single-strand RNA viruses [3]. This virus is responsible, in some susceptible individuals, of an acute respiratory syndrome, SARS, which is associated with clinical symptoms in the lower and upper respiratory tracts. One of the essential transmitting ways for the virus is through the air, which can be transported on air paths inside the room. During the respiratory activity, the droplets' size increases, and the actual size distribution of these droplets depends on parameters such as expiratory air velocity, fluid viscosity, and flow path [4]. Lippmann [5], using a hollow cast experimental method simulated the regional deposition of an inhaled particle in the human respiratory system and by considering the particle diameter between 0.2 to 7 microns concluded that aerosol particles' deposition efficiency with an aerodynamic diameter greater than 2 μm depends on the Stokes number. Nowak et al. [6] using two geometric models simulated airflow and aerosol deposition in the human tracheobronchial tree. Based on their findings, they concluded that the use of geometric models based on CT scan has more satisfactory results to simulate particle deposition. Therefore,

* Corresponding author: Hamidreza Mortazavy Beni. Department of Biomedical Engineering, Arsanjan Branch, Islamic Azad University, Arsanjan, Iran.
E-mail address: h.mortazavy@iaua.ac.ir (H.M. Beni).

https://doi.org/10.1016/j.cmpb.2020.105843
0169-2607/© 2020 Elsevier B.V. All rights reserved.

they used a CT scans simulation model and found that in airway intersections and the tubular walls, the deposition mechanism was more prevalent. On the other hand, Matida et al. [7] used the eddy interaction model to particle deposition and concluded that the kinetic velocity of the flow turbulent plays a significant role in the particle deposition. Heyder [8] concluded that in the human respiratory system, due to the inlet air forces applied to inhaled particles, their path differs from that of airflow lines. The most important mechanical forces applied to them include gravity, inertia, and impact transfer from molecular collisions. Therefore, the particles move from the flow lines and deposit on the surfaces of the respiratory tract. Zhang and Kleinstreuer [9] analyzed the transfer and deposition of nanoparticles in a steady flow in a model of the upper human airway. Like Heyder [8], they concluded that the regional deposition of nanoparticles in the 0.001-0.15 μm range could depend on the flow rate of inhalation, particle size, and geometric length scale. Mahesh et al. [10] developed a numerical algorithm to perform large eddy simulation (LES) in extraordinarily complex geometries such as the respiratory system geometry. This algorithm has been developed for unstructured hybrid grids, which is more suitable in high Reynolds numbers and highly skewed grids simulation. This algorithm is very efficient for a fine mesh with high Reynolds numbers. Zhou and Cheng [11] also found that deposition efficiency and Stokes number subordination, similar to Lipmann's research [5], depending on the other parameters, including the angle of intersection and the diameter of the tract. Also, the deposition of particles in the trachea depends on the type of flow in this area, which is turbulent due to the laryngeal jet. Jin et al. [12] simulated the deposition of inhaled particles in the human upper respiratory tract by the LES method. They then modeled a steady flow with three types of flow rates of 30, 60, and 90 L/min. The results showed that the growth of the diameter and density of particles and the intensity of respiration increased the deposition of particles in the upper human respiratory tract. Farkas et al. [13] investigated the local deposition patterns of therapeutic aerosols in the pharyngeal airways, healthy and diseased bronchi, and alveoli using computational fluid dynamics (CFD) and particle dynamics techniques. Their findings revealed that nanoparticle deposition patterns were more uniform than micro-particles in the entire respiratory tract at all flow rates. They also observed that the deposition of nanoparticles in the airway decreases with flow velocity increasing. However, in the case of micro-particles, deposition increases at high flow velocities. Xi and Longest [14] investigated the transport and deposition of micro aerosols in real models of the respiratory system with real dimensions and measures achieved from CT scans of a healthy adult. Eventually, they concluded that the low Reynolds number k-omega turbulent model was suitable for simulating particles with a diameter of 1 to 31 μm simplified geometry of the respiratory system. They also found that real geometries provided the best predictions of regional deposition compared to experimental data as a function of particle diameter. Shi et al. [15] studied the inertial particles in the diameter range of 1 to 50 μm, considering the steady laminar flow rate of 7.5 and 20 L/min, and concluded that the most deposition occurs in the anterior part of the nasal cavity. However, total deposition in the inferior meatus and olfactory areas is tiny due to the complex geometric structures of the nasal cavity. The results of the simulation of Li et al. [16], like other researchers [7, 9] in the upper human airway, demonstrate that the specific inlet velocities affect the particle deposition. They also found that kinematic upstream effects are significant for particle deposition, although they have less effect on the flow field. Due to the structures of the tracheal ring, the highest deposition occurs at a higher flow rate. The results of Lin et al. [17] as other studies Showed that a turbulent jet flow in the larynx occurs, while the intensity of turbulence in other airways is weak. Also, turbulence caused by the laryngeal jet can significantly affect the airway flow pattern as well as the shear stress of the tracheal wall. Jayaraju et al. [18] set the inhalation rate at 15, 30, and 60 L/min with a particle diameter between 2 and 20 μm. Their results revealed that more massive particles at lower flow rates cause more deposition than sediments at higher flow rates. Oral inhalation (15, 30, and 60 L/min) along with the deposition of aerosols with a diameter of 1-30 μm calculated by CFD using the K-epsilon turbulent model by Ma and Lutchen [19] similar to Jayaraju et al. method [18]. They found that more deposition was obtained from micrometer-sized aerosol particles. Their study represents an essential step in predicting subject-specific aerosol deposition throughout the lungs with the airways' real anatomical geometry. Mihai et al. [20] exploited two stable strategies to model the flow, including steady Reynolds-Averaged Navier-Stokes (RANS) and LES. Considerable differences in static pressure distribution in the air walls between LES and RANS data were observed in the pharynx cross-sectional area. Furthermore, it is revealed that the most considerable difference is in the downstream axial velocity distribution of the minimum cross-sectional area, which is characterized by flow separation and the large radial velocity gradient across the developed shear layers. An analysis of Shanley et al. [21] in a steady laminar flow illustrated that a simple uniform flow occurs in the nose with a peak in the speed, and a peak immediately occurs in the posterior part in the size of vorticity. The results of particle accumulation smaller than 10 μm through the Lagrangian method depicted that the deposition increases with larger particle size and flow velocity. In other studies conducted by Kleinstreuer and Zhang [22], the flows of a respiratory system can include turbulent jet with substantial pressure drop, while breathing in the airways. It was also found that micron particles were modeled in the Lagrange-Euler framework, and nanoparticles were modeled based on the Euler-Euler approach, preferably. Inthavong et al. [23] by numerically modeling of the nanoparticles' deposition in the nasal cavity and tracheobronchial airway found an upsurge in the deposition in the nasal cavity for nanoparticles, and in general, the deposition pattern spreads more through the airways. The use of nanoparticles creates a potential opportunity to improve drug delivery patterns and increase drug deposition in the middle turbinate regions of the nasal cavity where most mucosal walls are located. Huang and Zhang [24] by numerical simulation of micro-particle's deposition in respiratory system's real model during the transient breathing cycle concluded that the deposition is highly dependent on the rate of respiration less dependent on the turbulence of the flow. Particles are mainly distributed in high-velocity axial regions and follow the secondary flow. They also found that the transient deposition fraction strongly depends on breathing flow rate and particle diameter but is less affected by turbulence intensity. Frank et al. [25] using the computational fluid dynamics model of the human nose, recognized that speeds of more than 3 m/s slow down the particle's penetration in the respiratory system. Also, in the presence of septal deviation, a spray of 10 micrometers may have good penetration. Philip and Wang [26] believe that the complex geometry of the airway of the human respiratory system itself creates a continually changing hydrodynamic flow field. In this way, airborne particles during inhalation with the small amount of fraction deposition on the airway surfaces can penetrate different parts of the respiratory tract, and thus a variety of beneficial or hazardous substances can enter the body. Li et al. [27] findings indicate that the efficacy of micro-particle deposition is much higher than that of nanoparticles. The diameter of nanoparticles is less critical than that of micro-particles in the deposition. Also, the highest values of particle deposition efficiency and deposition concentration both occur in the nasal cavity, while the highest capture efficiency up to 99.5% occurs in the bronchus. Yousefi et al. [28], like other researchers [11, 12, 17], found that the most

particle deposition exists in the larynx, where the airways have a smaller cross-sectional area. Also, as Mihai et al. [20] showed, particle deposition patterns in airways depend on their initial inlet position at the mouth inlet. Varghese and Gangamma [29] believe that the presence of water droplets in the inhale can alter the size of inhaled aerosols. Therefore, they could change the deposition profile of inhaled airborne particles in the lungs. However, the analytical method applied for particles with a diameter of more than 1 μm and high concentrations has a high computational error. Basu et al. [30] simulated airflow during respiration through a steady, viscous, and laminar model and found that such a method demonstrates a relative insensitivity to input disturbances. During their research, they concluded that the posterior airflow transport and trend of the particles deposition should not be affected by the nozzle subtraction and the vestibular dilation. Islam et al. [31] in the studies of sediment patterns showed that most aerosol particles are placed on the tracheal wall instead of the carina angle. At low flow velocity, particle density is mostly in the middle of the trachea. At higher flow velocity, particle density increases at the top region and in the path change region. Like other studies [12, 14, 18, 27], they concluded that particle diameter and fluid flow velocity affect the deposition pattern. Using the CFD simulation, they found that the effects of turbulence on deposition were more effective for larger diameter particles and less effective for smaller diameter particles. Using the CT-based model, they found that a significant amount of particle deposition settles on the tracheal wall, whereas in the simulation, it was observed that more particles precipitate at the carnival angle in the unreal model [32]. In general, it can be understood from the above researches that there is a great deal of difference in the findings due to the complex geometry of the respiratory system and the computational method used for particle deposition.

There is no investigation of viral effects performed about droplets smaller than 10 μm diameter, but even in vitro studies have not been performed to determine these droplets' exact deposition location in the upper human respiratory system. As mentioned in the literature review, avoiding the real model in the respiratory system can immensely affect particle deposition. Real geometry is fundamental in modeling, and computational methods based on actual body performance can affect the results. Unlike previous research, which examined the motion of particles by CFD, in this study, the FSI model is used because the body's physiological conditions behave as FSI manner.

2. Methods

2.1. Computational Model

The model used in this study is related to a 30-year-old healthy man who has been reviewed and approved in the past research in terms of CFD [33] and FSI [34], and has a very high level of reliability. In this model, the three-dimensional (3-D) model of the upper airway is extracted using CT technology. Then, three-dimensional geometry is constructed, including the nostril entrance to the carina (nasal cavity, pharynx, larynx, and trachea). It is very carefully segmented and meshed to create a computational grid, considering the appropriate boundary layer. After examining the grid's independence, this model has been made with an approximate number of 2.6 million computational nodes for mesh production. This computational grid has excellent quality, which could accurately predict the behavior of thyroid cartilage failure and brain damage in respiratory reflexes.

Details of reconstruction of geometry and meshing of this model have been presented in Mortazavy et al. study [33], and it is not mentioned here again. Fig. 1 shows the meshed geometry of the computational model. In this figure, the nasal cavity was divided into three parts: superior, middle and inferior turbinate. The volume of each area increases from top to bottom so that the superior turbinate has the most, and the inferior turbinate has the least volume. These areas have particular importance, so that they play an essential role in heat transfer, increase moisture, and filter inhalation air. What makes this division salient is that these areas are full of blood vessels which their vastness has changed with slight changes in temperature, humidity, physical activity, body position, and hormonal changes.

2.2. Governing Equations

Air was considered as a viscous and incompressible fluid. The governing equations for the quasi-steady turbulent flow based on Shanley et al. [21] in the human respiratory system are the Navier-Stokes and continuity equations. These equations include:

$$\frac{\partial U_i}{\partial x_i} = 0 \tag{1}$$

$$U_i \frac{\partial U_j}{\partial x_i} = -\frac{1}{\rho}\frac{\partial P}{\partial x_i} + \frac{\partial}{\partial x_i}\left[\nu\left(\frac{\partial U_i}{\partial x_j} + \frac{\partial U_j}{\partial x_i}\right) - \overline{U_i' U_j'}\right] + G_i \tag{2}$$

In these equations, the parameters U, ρ, P, ν, and G_i for air-fluid represent speed, density, pressure, kinematic viscosity, and gravity term, respectively. Also, i and j represent Cartesian coordinates. Based on Kleinstreuer and Zhang [22], the E-L method was selected as the best method to investigate the micro-droplet particle movement along with fluid. The equation of motion for the micro-droplet is as follows:

$$\frac{du_i^P}{dt} = \left(\frac{18\mu}{\rho^P d^2 C_c}\right)\left(U_i - u_i^P\right) + g_i + F_x \tag{3}$$

Also, μ, ρ^P, d, g_i, and F_x are viscosity, particle density, particle diameter, gravity term, and Brownian Force, respectively. Furthermore, in this equation, $\frac{dx_i}{dt} = u_i^P$. Also, C_c is the Cunningham correction factor, which is equal to:

$$C_c = 1 + \frac{2\lambda}{d}\left(1.257 + 0.4e^{-\frac{1.1d}{2\lambda}}\right) \tag{4}$$

In this equation, λ is the average molecular distance for air and was assumed to be 0.065 μm. The Stokes number was used to calculate the ratio of the droplet's characteristic time per the characteristic time scale of the flow, which is defined as follows.

$$St^P = \frac{\tau u_f}{d_c} \tag{5}$$

In which τ is the characteristic time, u_f is the velocity of the fluid, and d_c is the tract's hydraulic diameter through which the fluid passes. By putting the value of residence time, the following equation is obtained:

$$St^P = \frac{\rho^P d^2 u_f}{18\mu d_c} \tag{6}$$

The walls of the airway were considered as an elastic wall. It was also assumed that the droplets were absorbed in the first encounter with the wall. More details on the governing equations of FSI mentioned in the Mortazavy et al. study [34], are not repeated here for the sake of brevity. In the present model, based on Shanley et al. [21], the fixed boundary conditions, mouth and end of the trachea (carina zone) are where the flow rate enters and exits, respectively. In the numerical model, the flow rate entrance is from the mouth, and the wall boundary condition is applied to the nostril's entrance.

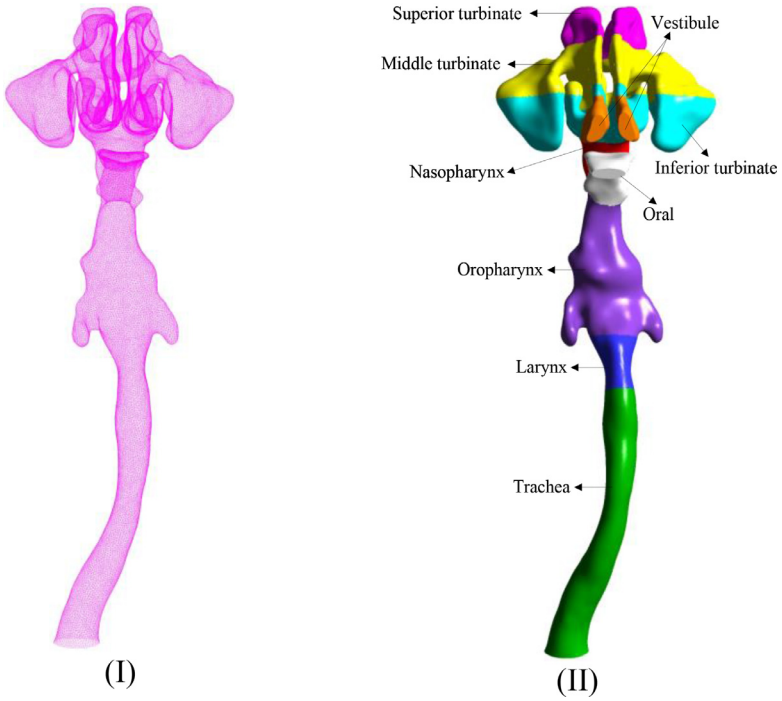

Fig. 1. Computational model geometry and meshing. (I) Numerical model meshing. (II) The geometry of the 3D model.

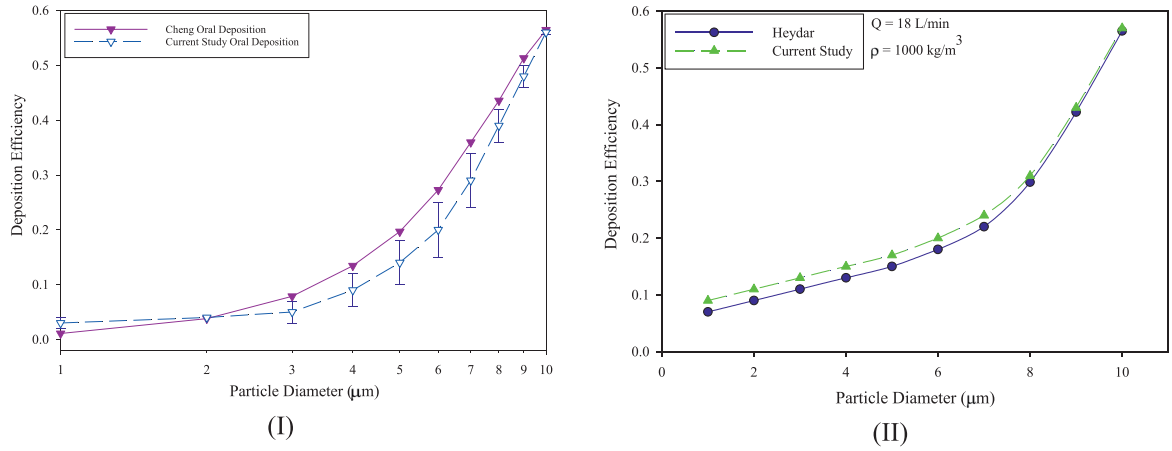

Fig. 2. Comparison of deposition efficiency towards particle diameter for the cheng and heydr results with the present model. (I) particles deposition in the inhalation through the mouth with the closed nose with an input flow rate of 30 L / min in the cheng study [37]. (II) Water droplet deposition in the oral inhalation at the inlet flow rate of 18 L / min in the heydar study [8].

2.3. Numerical solution and method verification

The geometry was entered into the fluent 6.3 software (ANSYS, USA). Fluent software converts and solves the governing equations into algebraic equations by the finite volume method. In this study, the second-order upwind scheme was used to the momentum equation discretization, and the SIMPLE algorithm was used to couple the pressure and velocity equations. The k-epsilon turbulence model is a subcategory of the RANS group, which has been shown to have viable results in the use of DPM in the study of deposition mapping in the human respiratory system [19]. That is why this method was used in this study, and the reliability of this method was confirmed, according to Fig. 2. In the simulation process, air entered the model at 25 °C from the mouth, and as shown below, three amount of density considered for droplets entering the model. Then, the deposition efficiency was assessed in each state. $\rho_1 = 998kg/m^3$ for pure water density, $\rho_2 = 1119kg/m^3$ equivalent to 50% water + 50% virus (average density), and $\rho_3 = 1240kg/m^3$ was assumed for net virus droplet, given that the COVID-19 virus belongs to the Betacoronavirus family, and the density of the Betacoronaviruses is approximately $\rho = 1240kg/m^3$ [35]. Also, the range of droplet diameter changes in normal conversation was considered from 1 to 10 μm. For the respiratory wall, the expansion of the Young's modulus and Poisson's ratio were considered in the range of $0.51\text{kpa} \leq E \leq 100.64\text{kpa}$ and $\vartheta = 0.3 - 0.45$, respectively [36].

In order to validate the present study, the results obtained by Cheng [37] in the field of high-density solid aerosol (Fig. 2(I)), and the findings from heydar study [8] regarding particle deposition with water density (Fig. 2(II)) were used. As can be seen in Fig. 2, the results show a similar trend. Of course, according to Fig. 2(II) due to the similarity between the type of boundary conditions and the airflow with the droplet type, a better match has been obtained. The reason for the incomplete overlap in the

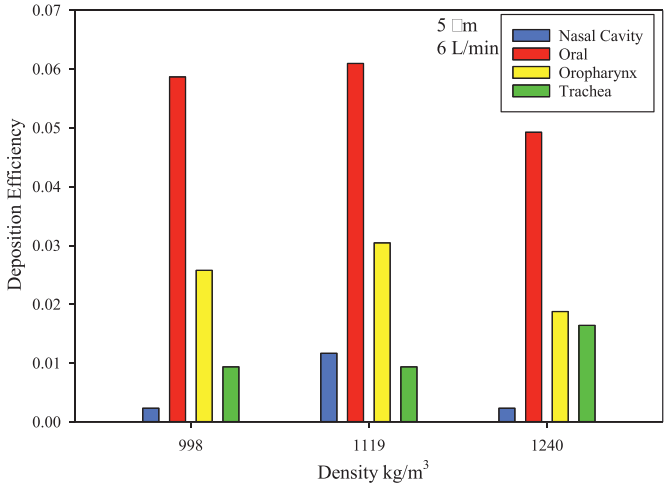

Fig. 3. Droplet deposition in the upper respiratory system regarding density at 5μm, 6L / min.

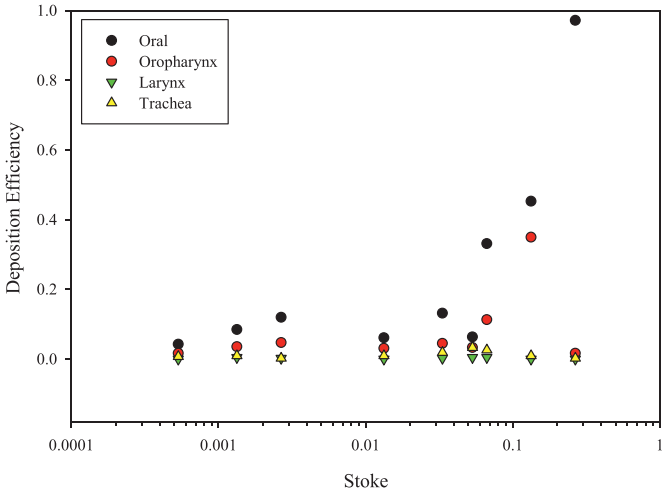

Fig. 5. Droplet deposition efficiency in different Stokes numbers.

results can be described in the difference between the analyzed geometries.

3. Results

In this study, flow inlet from the mouth with the closed nose, fluid flow, droplet parameters, and wall deformation analysis was investigated. Three flow rates of 6, 15, and 30 L/min were entered into the model along with the droplet diameter change, and based on this, the upper respiratory system's performance was evaluated from different aspects. Meanwhile, the flow rate of 6, and the 5 μm droplet diameter are the basis for comparisons. It should be noted that during normal breathing, a man in a state of rest breathes about 500cm^3 of air per inhalation, which is the same as the tidal volume at rest [38]. This number is precisely concordant with the model presented in this study after spirometry testing during patient health in the database [34]. Therefore, the inlet flow rate in the model was considered 6L/ min in rest mode.

3.1. Simulated airflow with droplet transport and deposition

Whereas, if the inhalation is done just through the mouth, based on Fig. 3, the highest droplet deposition in the different density changes occurs in the oral, oropharynx, and trachea, respectively. The deposition efficiency is smaller than 6%, which in the mouth is at least more than three times greater than the trachea.

According to Fig. 4, the most residence time occurred in the nasal cavity, so that it has the highest value in the superior turbinate during the mouth inhalation, with the difference in the number of droplets entering to this upper area of the nasal cavity. After this area, we should mention the amount of residence time in the trachea region, which is relatively significant. The most interesting issue is that residence time in oral and oropharynx is almost zero. Also, in general, it can be assumed that the amount of residence time is minimal, except in the nasal cavity.

According to Fig. 5, the highest droplet deposition in oral inhalation occurs in the oral and oropharynx, while the lowest in the larynx, and trachea, respectively. The amount of deposition in the mouth is significant and is often several times that of other respi-

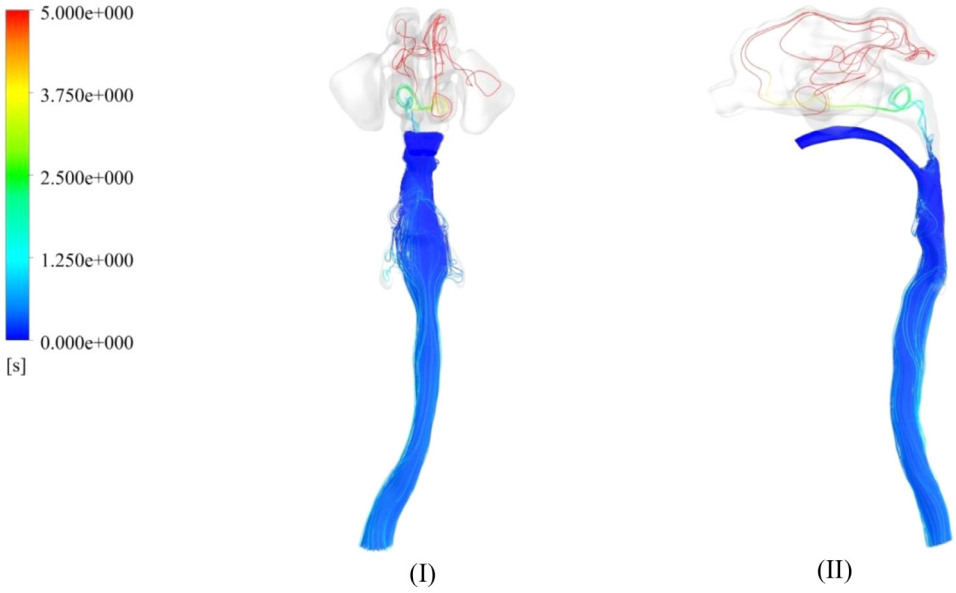

Fig. 4. Droplet residence contour with average density at 5μm diameter, and 6 L/min. (I) Droplet residence time tracking in the coronal plane. (II) Droplet residence time tracking in the sagittal plane.

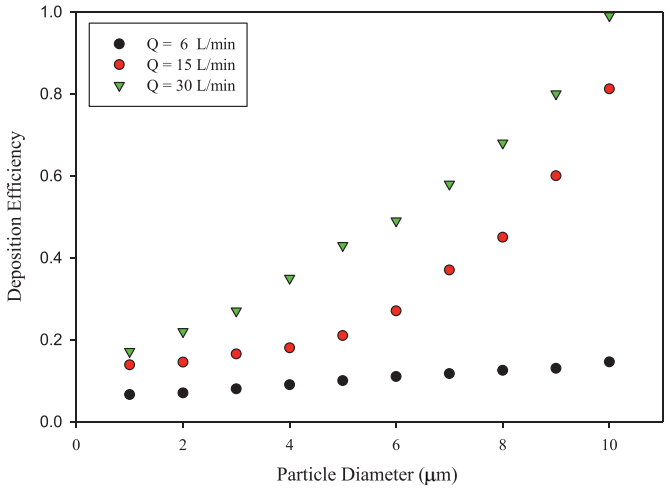

Fig. 6. Deposition efficiency in different droplet diameter, and flow rates at average density.

ratory areas. For small Stokes numbers (St << 1), the droplet residence time is short and is almost equal to the fluid response time. Therefore, droplets almost follow the same as the airflow field.

Deposition efficiency changes based on droplet diameter at different flow rates for average density are shown in Fig. 6. As can be seen, the amount of deposition increases with diameter or flow rate elevation. At a flow rate of 6L/ min, the total deposition efficiency in the range of droplet diameter changes from 1 to 10 μm is smaller than 20%, and the incremental slope of the curve is very slow. However, at the flow rates between 15 and 30 L/min, the deposition efficiency substantially increases with droplet diameter growth. This way, deposition efficiency is about 100% in 30 L/min flow rate and 10 μm diameter; in other words, no droplet enters the lungs.

Meanwhile, it is crucial to study the droplet mass concentration contours, as shown in Fig. 7, for accurate observation of droplet gathering regions. As can be seen from this figure, in mouth inhalation with a closed nose, the nasal cavity is filled with a minimal droplet concentration at the beginning of the flow. This low concentration can also cause deposition due to high residence time in the olfactory area and maxillary sinus (see Fig. 4).

3.2. Simulated solid domain deformation

Additionally, as can be seen from the presented deformation contour in Fig. 8, it is clear that the deformation in the mouth and nasal cavity is minimal, and the most deformation can be seen at the end of the trachea, near the carina. The maximum deformation rate at 15 and 30 L/min flow rates is 6, and 19 times greater than the 6 L / min flow rate. With a marginal increase in flow rate, the deformation rate would be several times greater.

4. Discussion

In order to get a more accurate answer, in a real model with the DPM method and with the FSI boundary condition in the wall at the time of inhalation, the droplets were injected into the respiratory system from the entrance of the mouth. Finally, a reliable model was developed, which, despite its complexity, has very reliable output responses and is consistent with the physiological behavior of the human body. Undoubtedly, tracking the viral droplet effects on the respiratory tract can help understand how to cope with and treat the disease. When an infected person exhales, many viral micro-droplets are produced, which can be suspended in the air and even move longer distances. Therefore, those in such an infected place inhale viral particles, and eventually, the disease spread faster. The basic mode of comparisons for the flow rate was considered 6 L/min; this number indicates the person's breathing rate in the rest position, and it is of great importance. It is more often that People in an indoor construction find themselves in such a situation, in which the risk of virus transmission through micro-droplets increases with improper ventilation. If a person starts moderate physical activity in the enclosed construc-

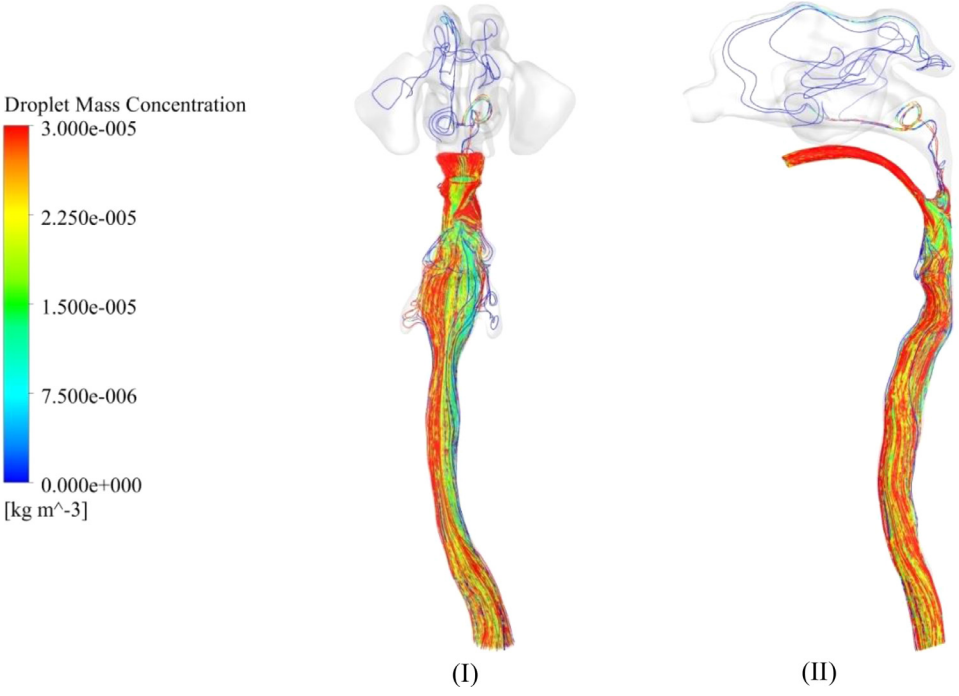

Fig. 7. Droplet mass concentration tracking contour for average density at 5 μm, and 6L / min. (I) Coronal plane tracking view, (II) Sagittal plane tracking view.

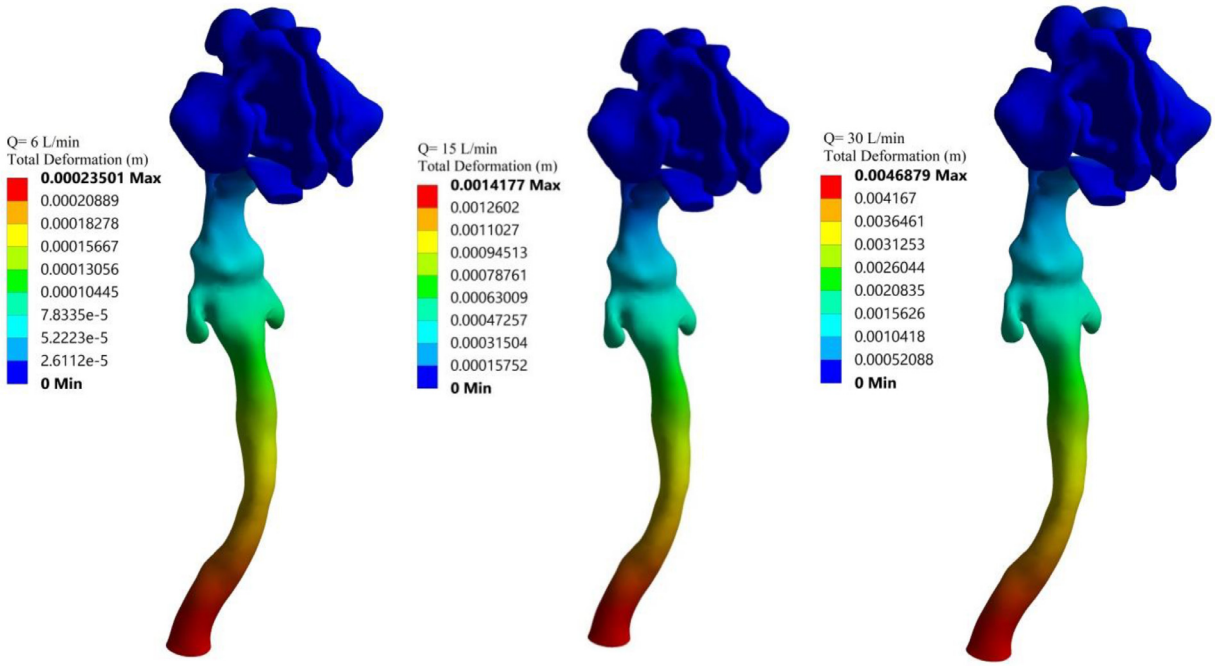

Fig. 8. Deformation contour at average density for different flow rates at 5μm droplet diameter.

Table 1
The Summary of the droplet deposition efficiency percentage with flow rate and droplet diameter changes in different areas of the upper respiratory system.

Condition		Percent of droplet deposition efficiency in each zone									Total	
Capacity	Size	Vestibule	Superior	Middle	Inferior	Nasopharynx	Oral	Oropharynx	Larynx	Trachea	Deposited	Escaped
6 L/min	1μm	0	0	0	0	0	4.23	1.64	0	0.70	6.57	93.43
	5μm	0	0.23	0.42	0.52	0	6.10	3.05	0	0.93	11.26	88.74
	10μm	0	0.17	0.33	0.67	0	6.34	3.30	0.47	3.29	14.56	85.44
15 L/min	1μm	0	0	0.21	0.25	0	8.45	3.52	0.47	0.93	13.84	86.16
	5μm	0	0	0.23	0.47	0	13.15	4.46	0.23	1.88	20.42	79.58
	10μm	0	0	0	0	0	45.31	34.98	0	0.94	81.23	18.77
30 L/min	1μm	0	0	0	0	0	11.97	4.69	0.23	0.23	17.12	82.88
	5μm	0	0	0	0	0	33.10	11.27	0.47	2.58	47.42	52.58
	10μm	0	0	0	0	0	97.18	1.64	0	0.23	99.05	0.95

tion, depending on the activity level, the flow rate results will be more practical at15 L/min and 30 L/min.

Some of the present study's limitations are presented as air inhaled through the mouth (closed nose) as well as constant number of injected droplets. The most deposition occurs in the mouth. The highest residence time occurs in the superior turbinate, which occurs with a low concentration. Also, according to Fig. 5, the larger Stokes number leads to higher deposition efficiency. This study's other achievements include increasing of the deposition efficiency by the droplet diameter and flow rate rise. Table 1 summarizes the deposition efficiency in the upper respiratory tract. So that the last two columns of this table present the percentage of total deposition and the percentage of output from the carina ring, and reached two lungs bronchi.

Droplet deposition pattern contour is presented at the 1,5,10 μm droplet diameters in the 30 L/min flow rate in Fig. 9, in which for better illustration, only droplet deposition areas were demonstrated. The droplet deposition increased in the oral cavity by droplet diameter growth, and therefore the less viral droplet reached the lungs. Only those droplets that reached the lungs, feasibly infect the person. This virus's receptor exists in the lungs across the inhalation path from mouth to the lungs [39]. Hence, the only way for the virus to transmit to the body in the 30 L/min airflow is through the lungs with a microdroplet smaller than 10 μm. When a person inhales through the mouth with the closed nose, not only the droplet deposition in the nasal area is almost zero, but other amounts of depositions in the mouth and throat can vanish with the mouthwash's help. Luise et al. [40] used eight types of mouthwash in pharmacies with different ingredients. In a laboratory, they combined these mouthwashes with the SARS-Cov-2 for 30 seconds by simulating the real oral environment and found that after 30 seconds, almost all coronaviruses disappeared.

Fig. 10, based on the last column of Table 1, shows a better view of the possibility of lung contamination. In all flowrates, if the size of the droplet is 1 μm, the probability of lung contamination will be more than 80%. By increasing the flow rate and droplet diameter, the process of lung contamination decreases so that for 10 μm droplet and 30 L/min airflow, the lung contamination is less than 1%. As, this virus's receptors are also active in the nasal cavity [39], it is recommended that the respirator masks should be made in such a way that the most air is inhaled through the mouth; so that in closed places where there is a high risk of virus contamination, the passage of air through the nose decreased. Hence, with the help of antiseptic mouthwash/gargling, the dose of the virus in the oral cavity and then in the upper respiratory system is significantly reduced.

Another essential point in this FSI model is that the most deformation can be seen in the carina zone, while the least droplet de-

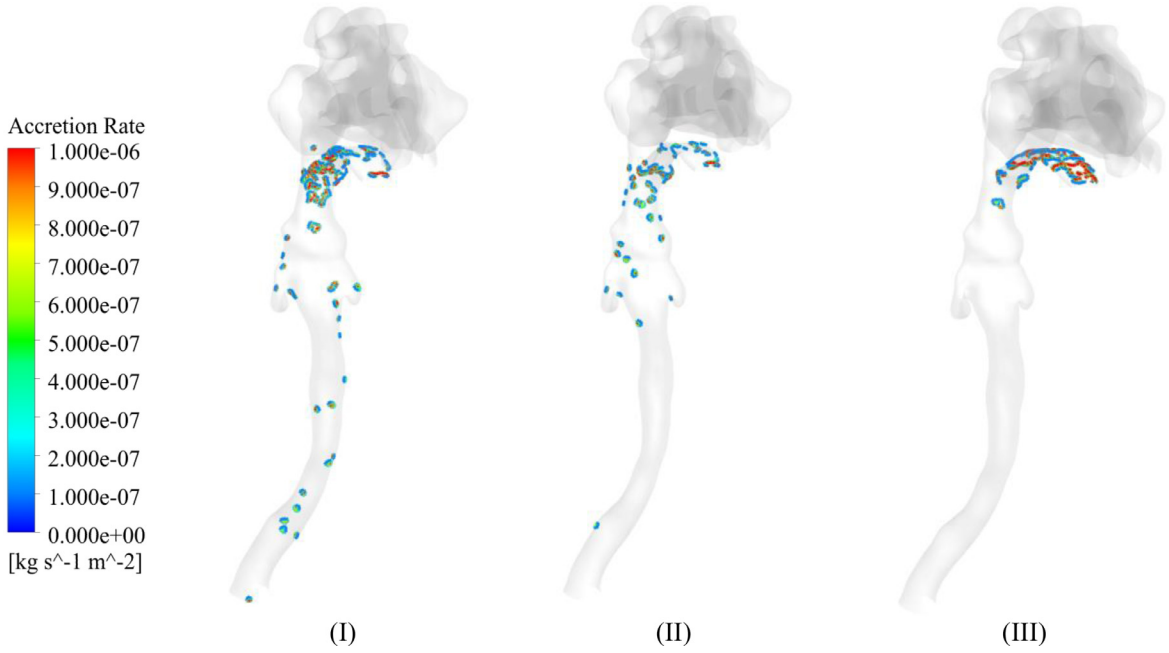

Fig. 9. Droplet deposition with 1, 5, and 10 μm droplet diameters at 30L/min airflow. (I) Mouth inlet 1µm droplet. (II) Mouth inlet 5µm droplet. (III) Mouth inlet 10µm droplet.

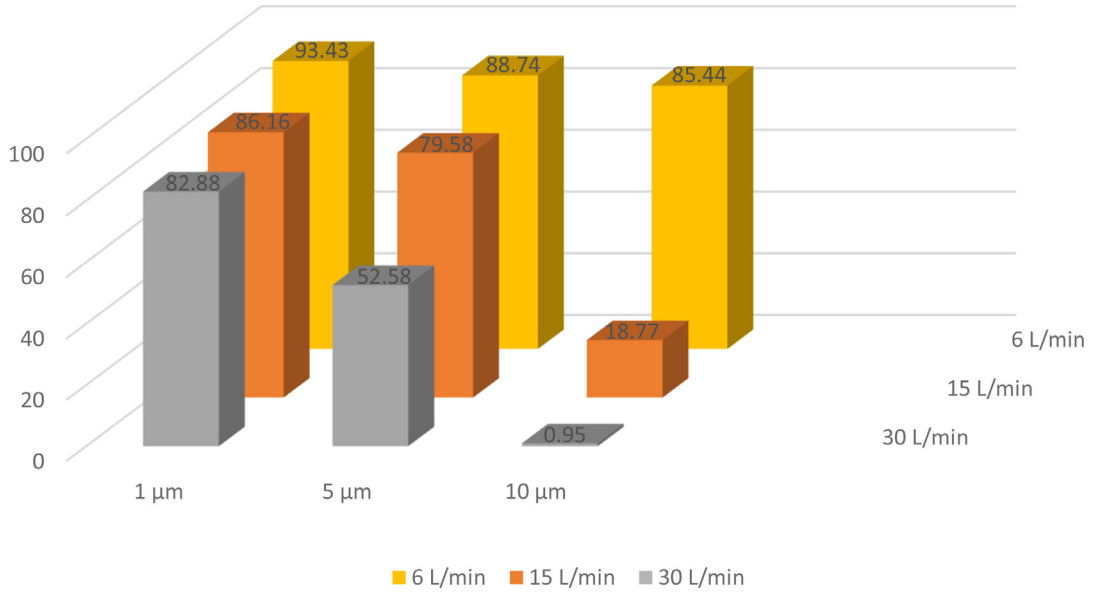

Fig. 10. Viral contamination probability percentage in oral inhalation for the droplet with 1, 5, and 10 μm diameters at 6, 15, and 30 L/ min airflow.

position occurs in these areas. It was confirmed by the CT [32] images that the droplet deposition at the carina angle is smaller than the trachea wall. Whereas in contrast, the result in unrealistic models is vice versa. Hence, the FSI method implementation in the analysis of droplet deposition in the upper human respiratory system is of great necessity to detect viral-infected areas accurately. In the model presented, the available volume from the carina to the nostril, regardless of the bronchus volume, is about 95 cm^3, which is part of the anatomic dead space and is in contact with the inner air surface of 329cm^2. This volume of the air is returned to the lungs after an exhalation during the next inhale. Therefore, if the anatomical dead space is contaminated with the virus, the droplet deposition residence time will increase significantly.

5. Conclusion

Utilization of a realistic model with accurate and precise computational analysis can end speculation about the deposition zone, accumulation, and the effects of the COVID-19 virus on the upper respiratory tract. On the other hand, recognizing the virus-containing droplet location can ease understanding the areas where the virus can first infect in the upper respiratory tract.

The previous studies on particle deposition in the human respiratory system suggested that each study's results depend on the particles' biomechanical nature and the chosen realistic computational method. In this study, droplets containing the virus were examined using the FSI method in a real human respiration geometry. We believe that to reach the exact answer, the model's geom-

etry must be authentic, and the FSI condition must be applied for the human model.

Although oral inhalation also causes contamination in the olfactory area, however, the virus concentration is deficient. Of course, this low concentration is trapped there due to the upper area's geometric structure, and because of the high residence time in this area, a percentage of it is absorbed, which is very small.

Declaration of Competing Interest

The authors of the manuscript hereby declare that they have no conflict of interests. The research was not funded by any organization or university.

Acknowledgments

We thank the Taba-Parto Shiraz radiology center for assistance with the 3D CT scan. All procedures performed in studies involving human participants were in accordance with the institutional and/or national research committee's ethical standards and with the 1964 Helsinki declaration and its later amendments or comparable ethical standards. The authors of the manuscript declare that they have no conflict of interest. Any organization or university did not fund the research.

References

[1] D.A.J. Tyrrell, M.L. Bynoe, Cultivation of a Novel Type of Common-cold Virus in Organ Cultures, Br Med J 1 (5448) (1965) 1467–1470.
[2] E.Y.C. Shiu, N.H.L. Leung, B.J. Cowling, Controversy around airborne versus droplet transmission of respiratory viruses: implication for infection prevention, Curr Opin Infect Dis 32 (4) (2019) 372–379.
[3] J. Gu, C. Korteweg, Pathology and pathogenesis of severe acute respiratory syndrome, Am J Pathol 170 (4) (2007) 1136–1147.
[4] YG Li, AT Chwang, WH Seto, PL Ho, PL Yuen, Understanding droplets produced by nebulisers and respiratory activities, Hong Kong Med J 14 (Suppl 1) (2008) S29–S32.
[5] T.L. Chan, M. Lippmann, Experimental measurements and empirical modelling of the regional deposition of inhaled particles in humans, Am. Ind. Hyg. Assoc. J. 41 (1980) 399.
[6] N. Nowak, P.P. Kakade, A.V. Annapragada, Computational fluid dynamics simulation of airflow and aerosol deposition in human lungs, Ann Biomed Eng 31 (4) (2003) 374–390.
[7] E.A. Matida, et al., Improved numerical simulation of aerosol deposition in an idealized mouth–throat, Journal of Aerosol Science 35 (1) (2004) 1–19.
[8] J. Heyder, Deposition of inhaled particles in the human respiratory tract and consequences for regional targeting in respiratory drug delivery, Proc Am Thorac Soc 1 (4) (2004) 315–320.
[9] Z. Zhang, C. Kleinstreuer, Airflow structures and nano-particle deposition in a human upper airway model, Journal of Computational Physics 198 (1) (2004) 178–210.
[10] K. Mahesh, G. Constantinescu, P. Moin, A numerical method for large-eddy simulation in complex geometries, Journal of Computational Physics 197 (1) (2004) 215–240.
[11] Y. Zhou, Y.-S. Cheng, Particle Deposition in a Cast of Human Tracheobronchial Airways, Aerosol Science and Technology 39 (6) (2005) 492–500.
[12] H.H. Jin, et al., Large eddy simulation of inhaled particle deposition within the human upper respiratory tract, Journal of Aerosol Science 38 (3) (2007) 257–268.
[13] A Farkas, I Balashazy, K Szocs, Characterization of regional and local deposition of inhaled aerosol drugs in the respiratory system by computational fluid and particle dynamics methods, J Aerosol Med 19 (2006) 329–343.
[14] J. Xi, P.W. Longest, Transport and deposition of micro-aerosols in realistic and simplified models of the oral airway, Ann Biomed Eng 35 (4) (2007) 560–581.
[15] H. Shi, C. Kleinstreuer, Z. Zhang, Modeling of inertial particle transport and deposition in human nasal cavities with wall roughness, Journal of Aerosol Science 38 (4) (2007) 398–419.
[16] Z. Li, C. Kleinstreuer, Z. Zhang, Simulation of airflow fields and microparticle deposition in realistic human lung airway models. Part II: Particle transport and deposition, European Journal of Mechanics - B/Fluids 26 (5) (2007) 650–668.
[17] C.L. Lin, et al., Characteristics of the turbulent laryngeal jet and its effect on airflow in the human intra-thoracic airways, Respir Physiol Neurobiol 157 (2-3) (2007) 295–309.
[18] S.T. Jayaraju, et al., Fluid flow and particle deposition analysis in a realistic extrathoracic airway model using unstructured grids, Journal of Aerosol Science 38 (5) (2007) 494–508.
[19] B. Ma, K.R. Lutchen, CFD simulation of aerosol deposition in an anatomically based human large-medium airway model, Ann Biomed Eng 37 (2) (2009) 271–285.
[20] M. Mihaescu, et al., Large Eddy Simulation and Reynolds-Averaged Navier-Stokes modeling of flow in a realistic pharyngeal airway model: an investigation of obstructive sleep apnea, J Biomech 41 (10) (2008) 2279–2288.
[21] K.T. Shanley, et al., Numerical simulations investigating the regional and overall deposition efficiency of the human nasal cavity, Inhal Toxicol 20 (12) (2008) 1093–1100.
[22] C. Kleinstreuer, Z. Zhang, Airflow and Particle Transport in the Human Respiratory System, Annual Review of Fluid Mechanics 42 (1) (2010) 301–334.
[23] K. Inthavong, K. Zhang, J. Tu, Numerical modelling of nanoparticle deposition in the nasal cavity and the tracheobronchial airway, Comput Methods Biomech Biomed Engin 14 (7) (2011) 633–643.
[24] J. Huang, L. Zhang, Numerical simulation of micro-particle deposition in a realistic human upper respiratory tract model during transient breathing cycle, Particuology 9 (4) (2011) 424–431.
[25] D.O. Frank, et al., Effects of anatomy and particle size on nasal sprays and nebulizers, Otolaryngol Head Neck Surg 146 (2) (2012) 313–319.
[26] Hopke, P.K. and Z. Wang, Particle Deposition in the Human Respiratory Tract, in Fine Particles in Medicine and Pharmacy. 2012. p. 223-240.
[27] D. Li, et al., Numerical Simulation of Particles Deposition in a Human Upper Airway, Advances in Mechanical Engineering 6 (2015).
[28] M. Yousefi, K. Inthavong, J. Tu, Microparticle Transport and Deposition in the Human Oral Airway: Toward the Smart Spacer, Aerosol Science and Technology 49 (11) (2015) 1109–1120.
[29] S.K. Varghese, S. Gangamma, Particle deposition in human respiratory system: deposition of concentrated hygroscopic aerosols, Inhal Toxicol 21 (7) (2009) 619–630.
[30] S Basu, DO Frank-Ito, JS Kimbell, On computational fluid dynamics models for sinonasal drug transport: Relevance of nozzle subtraction and nasal vestibular dilation, International Journal for Numerical Methods in Biomedical Engineering 34 (4) (2017) e2946.
[31] M.S. Islam, et al., Euler–Lagrange approach to investigate respiratory anatomical shape effects on aerosol particle transport and deposition, Toxicology Research and Application 3 (2019).
[32] M.S. Islam, et al., Euler-Lagrange Prediction of Diesel-Exhaust Polydisperse Particle Transport and Deposition in Lung: Anatomy and Turbulence Effects, Sci Rep 9 (1) (2019) 12423.
[33] H. Mortazavy Beni, K. Hassani, S. Khorramymehr, In silico investigation of sneezing in a full real human upper airway using computational fluid dynamics method, Comput Methods Programs Biomed 177 (2019) 203–209.
[34] H. Mortazavy Beni, K. Hassani, S. Khorramymehr, Study of the sneezing effects on the real human upper airway using fluid–structure interaction method, Journal of the Brazilian Society of Mechanical Sciences and Engineering 41 (4) (2019).
[35] Decaro, N., Betacoronavirus‡, in The Springer Index of Viruses, C. Tidona and G. Darai, Editors. 2011, Springer New York: New York, NY. p. 385-401.
[36] M.J. Birch, P.D. Srodon, Biomechanical properties of the human soft palate, Cleft Palate Craniofac J 46 (3) (2009) 268–274.
[37] Y.S. Cheng, Aerosol Deposition in the Extrathoracic Region, Aerosol Sci Technol 37 (8) (2003) 659–671.
[38] Cameron, J.R., J.G. Skofronick, and R.M. Grant, Medical Physics: physics of the body. 1992: Medical Physics Publishing Corporation.
[39] A.M. Baig, et al., Evidence of the COVID-19 Virus Targeting the CNS: Tissue Distribution, Host-Virus Interaction, and Proposed Neurotropic Mechanisms, ACS Chem Neurosci 11 (7) (2020) 995–998.
[40] T Luise Meister, Y Brüggemann, D Todt, C.A. Conzelmann, J Müller, R Groß, J Münch, A Krawczyk, J Steinmann, J Steinmann, S Pfaender, E. Steinmann, Virucidal efficacy of different oral rinses against SARS-CoV-2, The Journal of Infectious Diseases (2020) jiaa471 https://doi.org/10.1093/infdis/jiaa471 .